JOURNAL OF OPTOELECTRONICS AND ADVANCED MATERIALS, Vol. 12, No. 6, June 2010, p. 1343 - 1349

Surface topography and optical properties of nitrogen doped ZnO thin films formed by radio frequency magnetron sputtering on fused silica substrates

M. NICOLESCU, M. ANASTASESCU, S. PREDA, J.M. CALDERON-MORENO, H. STROESCU, M. GARTNER*, V. S. TEODORESCU[a], A.V. MARALOIU[a], V. KAMPYLAFKA[b], E. APERATHITIS[b], M. MODREANU[c]
Institute of Physical Chemistry, Romanian Academy, Spl. Independentei 202, 060021 Bucharest, Romania
[a]*National Institute of Material Physics, 105 bis Atomistilor Street, 077125 Bucharest – Măgurele, Romania*
[b]*FORTH-IESL, Crete, Greece*
[c]*Tyndall National Institute, University College Cork, Cork, Ireland*

We report here on the nitrogen doped ZnO (ZnO:N) thin films deposited by radio frequency (rf) magnetron sputtering using ZnN target (99.9% purity) on, unintentionally heated, fused silica substrates. After deposition Rapid Thermal Annealing (RTA) at 400 and 550°C for 1min in N_2 ambient have been performed on the ZnO:N thin films. The RTA impact on the optical and microstructural properties of ZnO:N thin films have been investigated by X-ray diffraction, Atomic Force Microscopy, Scanning and Transmission Electron Microscopy coupled with Energy Dispersive X-ray analysis, UV-VIS-NIR spectrophotometry and UV-VIS-NIR-Far IR Spectroscopic Ellipsometry. XRD and AFM results revealed an improvement in the crystalline state of ZnO:N and a reduction in the films surface roughness following RTA. The EDX spectrum showed the presence of the nitrogen in small quantities in the ZnO structure (nitrogen/oxygen=1/8). The optical constants of ZnO:N from UV down to Far IR spectral range together with the infrared active modes for ZnO:N are also reported.

(Received June 8, 2010; accepted June 16, 2010)

Keywords: N doped ZnO, Magnetron sputtering, Atomic Force Microscopy, X-ray diffraction, Scanning Electron Microscopy, Transmission Electron Microscopy, Energy Dispersive X-ray analysis, UV-VIS-NIR and IR ellipsometry

1. Introduction

Zinc oxide (ZnO) is an optically transparent material of technological importance for, among other things, its use as a transparent conducting oxide in flat-panel displays and solar cells, and its potential as a blue-light-emitting diode. ZnO is a wide band-gap material ($E_g \approx 3.37$ eV) with large exciton binding energy $E_{ex} \approx 60$ meV at room temperature [1], which makes it feasible for optoelectronic devices [2] light-emitting devices [3], gas sensor [4], solar cells [5], transistor [6] and photocatalysts operating in the UV range. The use of the ZnO in these applications requires the ability to control the majority-carrier type and concentration. Although the growth of n-type ZnO [7, 8] is straightforward, p-type doping [9] has proven significantly more difficult. Theoretical calculations of the electrical behavior of defects, impurities, and single atomic species such as nitrogen predict difficulty in attaining p-type ZnO [10–14]. Despite these predicted difficulties, experimental evidence shows that p-type ZnO can be grown using a single intentionally added acceptor species, with nitrogen being the most common [15].

In this paper we investigate the optical and microstructural properties of nitrogen doped ZnO (ZnO:N) thin films formed on fused silica substrates by radio frequency magnetron sputtering. We report here also on the impact on the post deposition Rapid Thermal Annealing on the physical properties of ZnO:N thin films.

2. Experimental

2.1 Film preparation

The ZnO:N thin films were deposited by rf magnetron sputtering using ZnN target (99.9% purity) on, unintentionally heated, fused silica substrates. The substrates were ultrasonically cleaned in acetone and isopropanol, rinsed in deionizer water and dried in flowing nitrogen gas. Prior deposition, the target was pre-sputtered for at least 15min (Ar plasma, 5mTorr, 100 W rf-power) to remove any contaminants from the target surface and to enable equilibrium conditions to be reached. The rf-power was kept at 100W the ratio of gases flow rates was $Ar:O_2:N_2$=5:4:1 and the total pressure was 5mTorr. Following deposition, the ZnO samples were treated by Rapid Thermal Annealing (RTA) for 1min in N_2 atmosphere, at 400 and 550°C.

2.2. Characterization methods

The X-ray diffraction (**XRD**) measurements were performed using Rigaku Ultima IV equipment, with Cu Kα radiation and a fixed power source (40 kV and 30 mA). The diffractometer was set in condition of grazing incident X-ray diffraction (GIXD) with ω= 0.5°. The films were scanned at a rate of 5° (2θ)/min over a range of 5-90°. Crystallites sizes were obtained from the Scherer's

formula with the peak assignments given by the software machine.

Atomic force microscopy (**AFM**) measurements were performed in order to examine the surface morphology. EasyScan2 model from Nanosurf® AG Switzerland instrument was employed with a high resolution scanner of 10 μm ×10 μm ×2 μm working in the intermittent-contact and contact modes and by using sharp tips (radius of curvature of less than 10 nm) from Nanosensors™. SPIP™ software package (v. 4.6.0.0) was used to evaluate the dimension the superficial grains by using the so-called watershed method with gradient norm [technical details available on www.imagemet.com]. Additional information on the ZnO:N thin film morphology have been obtain using Jeol JSM-840 Scanning Electron Microscope (**SEM**).

The UV-VIS-NIR Perkin Elmer Lambda 950 spectrophotometer was used for the normal incidence **transmission measurement.**

Transmission Electron Microscopy (**TEM**) coupled with Energy Dispersive X-ray (**EDX**) measurements were performed on specimens extracted from the films [16] using a Jeol 200CX electron microscope. Spectroscopic ellipsometry (**SE**) measurements were performed on a large spectral range with Woollam equipment composed by a VASE ellipsometer for UV-VIS - NIR range and a rotating-compensator infrared spectroscopic ellipsometer for IR spectral range (**IR-SE**). Measurements have been performed using the 70° as incidence angle both for UV-VIS - NIR and IR spectral range.

3. Results and discussion

3.1 XRD

The diffraction pattern for as deposited and post deposition RTA ZnO:N samples is shown in Figure 1.a. All the peaks can be assigned to the ZnO wurtzite-type structure according to JCPDS data card 36-1451. The peak located at 2θ = 34.25° indicates that the (002) orientation dominates in ZnO:N films deposited on fused silica. Regular position of (002) ZnO line according to JCPDS standard is 34.44°. This line displacement is accompanied with the lattice strains which are present in the ZnO:N films due to lattice mismatch between the layer and substrate [17].

Following RTA the Full Width at Half Maximum (FWHM) of the (002) peak decreases (see Table 1) and the (002) reflection becomes more intense (see Fig. 1.b) at 550°C relative to 400°C. These demonstrates that the crystalline state of the ZnO:N thin films is improved upon RTA. Moreover, as is shown in Table 1 the crystalline grain size increases following RTA at 400 and 500°C (1min on N_2).

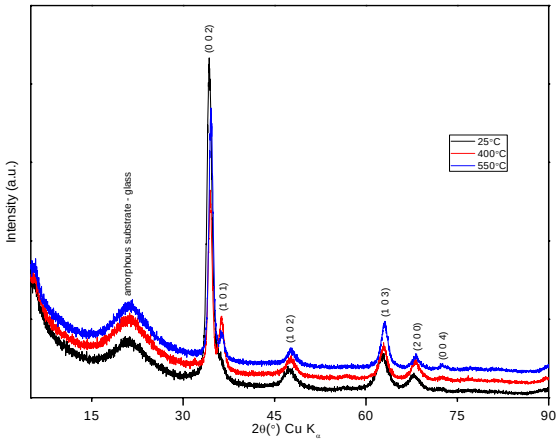

Fig. 1a XRD patterns for ZnO:N films deposited on fused silica before (25°C) and after RTA at 400 and 500°C (1min on N_2)

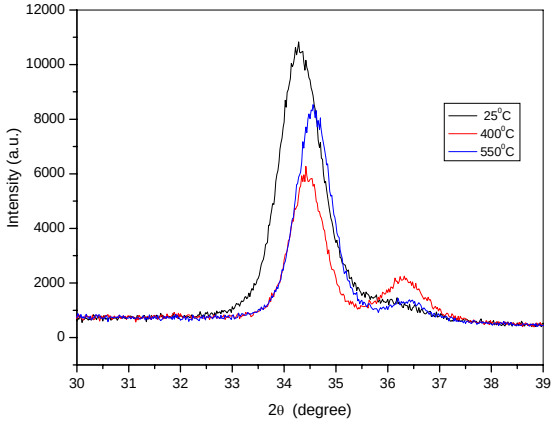

Fig. 1b The evolution of (002) peak following RTA at 400 and 500°C (1min on N_2)

Table 1. Crystalline grain size and position of the main diffraction peak for as-deposited and RTA (400 and 550°C) ZnO:N films.

Sample	(hkl)	2θ (degree)	FWHM (degree)	Crystallite size (nm)
25°C	(002)	34.25	0.92	9.35±0.1
400°C	(002)	34.37	0.76	11.31±0.1
550°C	(002)	34.54	0.78	11.09±0.1

Table 2. X-ray diffraction data of the crystalline ZnO:N thin film (our work and published data [18]).

(hkl)	d (Å)			d (Å) [18]
	25^{0}C	RTA 400^{0}C	RTA 550^{0}C	350^{0}C
(002)	2.6±0.13	2.6±0.13	2.5±0.12	2.5788
(101)	-	2.4±0.12	2.4±0.12	2.4546
(102)	1.9±0.09	1.9±0.09	1.9±0.09	1.8984
(103)	1.4±0.07	1.4±0.08	1.4±0.08	1.4709
(200)	1.3±0.06	1.3±0.07	1.3±0.08	-
(004)	-	-	1.3±0.07	-

3.2. AFM-surface topography

The AFM image of the as-deposited ZnO film (Figure 2a – 2D topographic view) reveals the columnar growth of the material which consists in well-separated crystalline particles disposed in the preferential c-axis and having a Root Mean Squared (RMS) roughness of about 5 nm. This is supported by diffraction peaks corresponding to the ZnO (002) orientation which is predominant, indicating that the films exhibit the c-axis preferential orientation. As a result, the grains are mainly grown with c-axis perpendicular to the substrate. After RTA at 400^{o}C (see Figure 2b) the surface of ZnO:N thin film reorganizes, being covered with nano-sized particles (30-100 nm) and presents some random distributed pores. When the RTA temperature increases to 550^{o}C there is further reorganization of the ZnO:N thin film that leads to a compact and homogeneously distributed grain structure with a mean diameter of 40 nm (see Figure 2c). When comparing the AFM results with the bulk crystallite size inferred from the XRD measurements (see Table 1) it could be seen that surface grains appear to be larger. From Figure 2 we can observe that following RTA the surface roughness of the ZnO:N films decreases. No major structural defects (cracks or exfoliations) were seen by AFM.

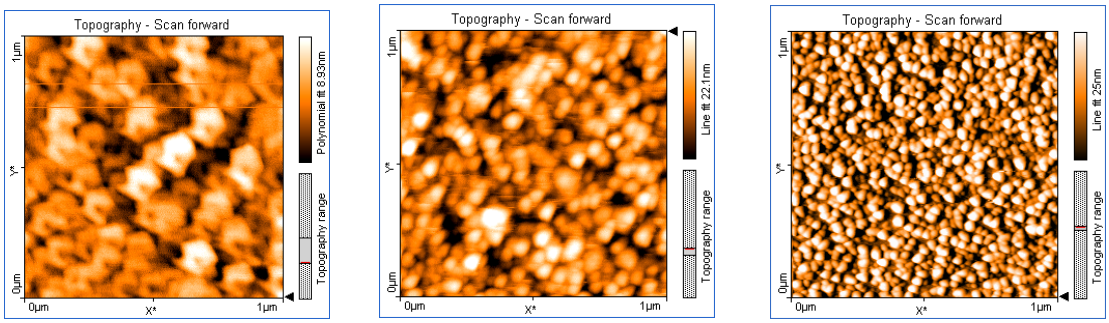

(a) (b) (c)

As deposited, RMS = 5.15nm **RTA-400^{o}C**, RMS = 3.87 nm **RTA-550^{o}C**, RMS = 4.76 nm

Fig. 2. Topographic images measured in different points at different scales revealing the morphology of the ZnO:N/fused silica films at nanometric scale.

3.3. SEM- global surface topography

SEM observations demonstrated a complete coating of the substrates. The Figure 3 and 4 show the morphology of coatings of ZnO:N as-deposited and after RTA at 550°C (1min on N_2). The observed morphology after deposition corresponds to dense polycrystalline films over the whole coated surface, in as deposited and thermally treated samples. Some irregularity in the deposition of materials is visible at large scales, forming a hills-like morphology, while the fine grain structure is observed in higher magnification micrographs.

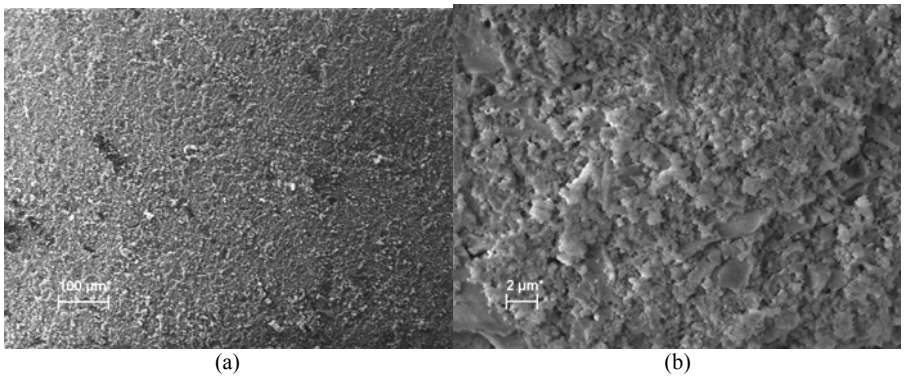

(a) (b)

Fig. 3. SEM micrographs of the as-deposited ZnO:N film at different magnifications, showing (a) the general morphology of a wide region and (b) the grain morphology of the polycrystalline coating .

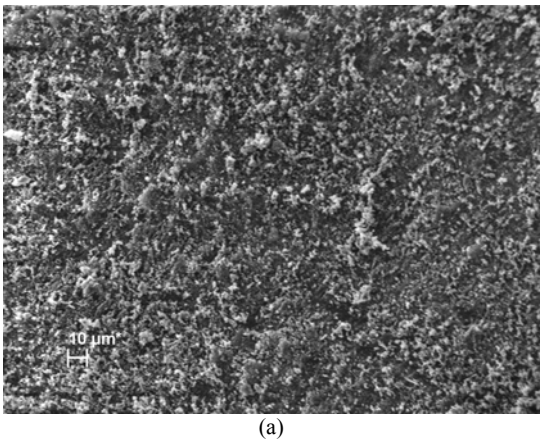

(a)

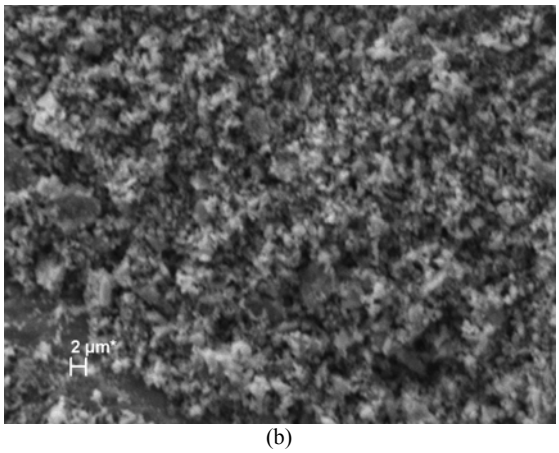

(b)

Fig. 4. SEM micrographs of the ZnO:N film after RTA at 550°C at different magnifications, showing (a) the general morphology and (b) the grain morphology of the polycrystalline coating.

3.4. TEM and EDX results

Fig. 5 shows the plan view TEM image of the film extracted from the substrate and the corresponding SAED pattern. The complete missing of the 002 reflexion in the SAED pattern (which is positioned between the 100 and the 101 reflexion of the ZnO structure) shows clearly the <001> texture of the film, orientation which is very common for the ZnO films grown by rf method. The Bragg contrast in the TEM image in Fig. 5 reveals crystallite dimensions between 10 and 40 nm, smaller than the AFM data. This was observed also for similar films deposited on silicon wafers [19] and is related mainly by the presence of the high stress field in the film. In these conditions, the grains revealed by AFM are composed by several nanocrystalline blocks with different orientation.

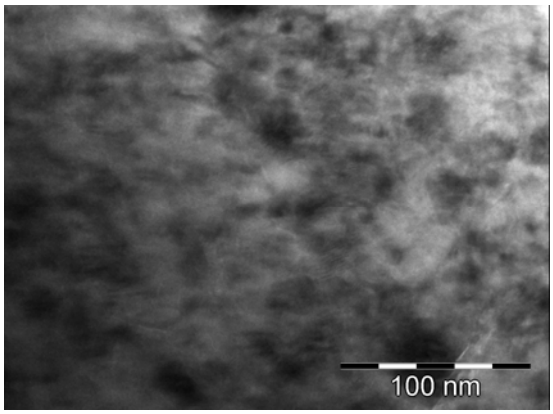

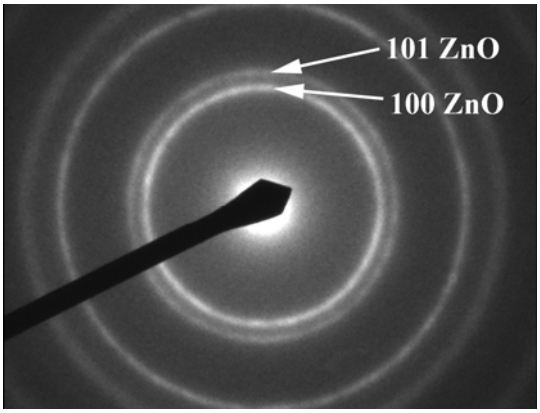

Fig. 5. Plan view TEM image and the corresponding SAED pattern of the ZnO:N film RTA at 550°C

The EDX spectrum acquired for the ZnO:N film RTA at 550°C (see Figure 6) shows the presence of the nitrogen in small quantities in the ZnO structure. The compositional calculations from such a spectrum, results a ration of about 1/8 between the nitrogen and oxygen.

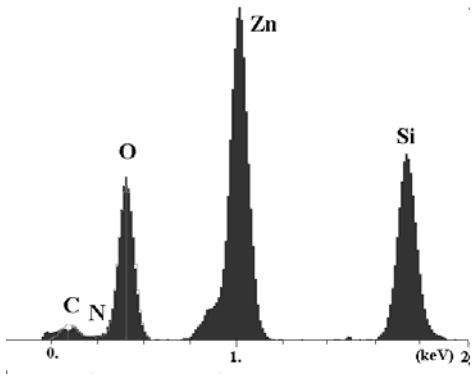

Fig. 6. Details of the EDX spectrum measured for the ZnO:N film RTA at 550°C, showing the presence of nitrogen.

3.5. UV-VIS-NIR spectrophotometry

In Fig 7 are shown the transmission spectra of the ZnO:N thin films as deposited and after RTA. Also in Figure 7 are plotted for comparison the transmission of a bare fused silica and a monocrystalline ZnO substrate. The films ZnO:N (in as deposited state and after RTA) are highly transparent in visible to NIR spectral range which is important for its application such a transparent conductive oxide (TCO) films and solar cell windows [20]. The absorption edge of the ZnO:N films is blue-shifted in report to that of bulk monocrystal ZnO and its evolution after RTA is in agreement with previous literature results [21]. The red-shift of the ZnO:N thin films following RTA is indicative of the optical band gap decrease. We can conclude that the increase of the film crystallinity after RTA leads to a slight decrease in the optical band gap, in agreement with the work of Dikovska et al. [22]. This also correlates with the Spectroscopic Ellipsometry findings in the Section 3.6.

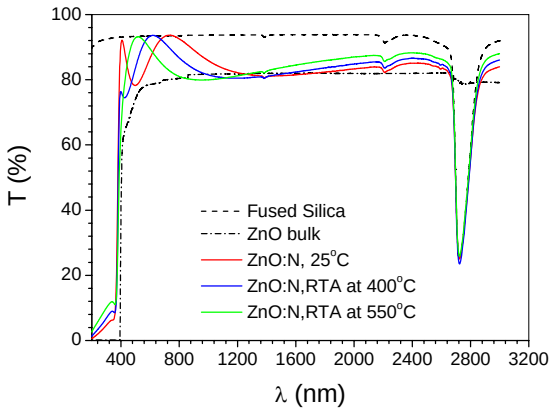

Fig.7.Transmittance spectra of rf sputtering ZnO:N films in comparison with fused silica and ZnO bulk spectra

3.6 Spectroscopic ellipsometry

3.6.1. UV-VIS-NIR

The evolution of the two ellipsometric parameters (ψ and Δ) with the RTA temperature is shown in the Figure 8.a and 8.b. A three-layer model (air/ surface roughness layer/ZnO film/fused silica substrate) was used for modeling the ellipsometric data. The agreement between measured and computed data is shown in the Fig.8a, b. The optical constants resulted from the best fit are presented in the Fig.8c,d. The thickness and the band gap value (computed by Tauc formula [23]) of as deposited and RTA films are presented in the Table 3.

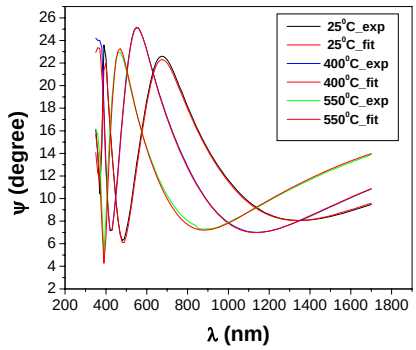

(a)

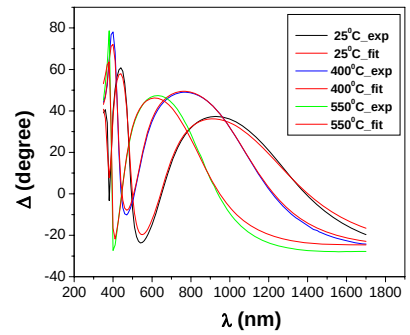

(b)

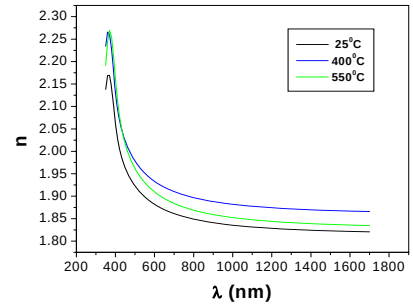

(c)

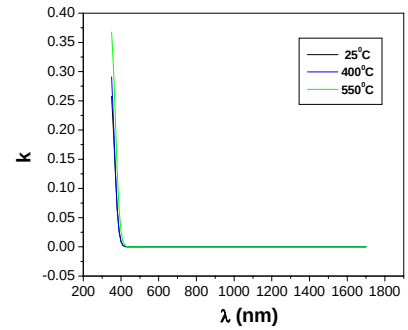

(d)

Fig.8 Ellipsometric results of ZnO:N films in the UV-VIS-NIR range for as-deposited and RTA films: (a,b)- the agreement between the measured and computed data of ψ and Δ spectra for all sample; (c,d) –optical constants constants

Table 3. Thickness (d_{film}), surface roughness ($d_{roughness}$) and band gap (Eg) values of ZnO:N films

Sample	d_{film} (nm)	$d_{roughness}$ (nm)	Eg (eV)
As-deposited	200.1	17.1	3.274
400	145.8	31.6	3.260
550	123.0	17.9	3.250

We can observed that the roughness values obtained by SE are larger than the RMS-AFM values (see Section 3.2) as the SE measurements integrate a much larger area (6mm^2) when compared with the AFM measurements (64 μm^2).

3.6.2 IR-SE

The ellipsometric parameters (ψ, Δ) of the fused silica substrate and of the as-grown and RTA films in the 300-1500 cm^{-1} are comparatively shown in the Figure 9.a and 9. b. The calculated data were obtained using three-layer model (air/surface roughness layer/ZnO:N_film/fused_silica substrate). A good agreement was obtained between the measured and calculated data for all samples (in Fig.9 c,d are exemplified the data for the ZnO:N film after at RTA 550^{0}C).

Fig. 9 e presents the imaginary part of the dielectric loss functions [Im(-ε^{-1})] for all three samples with a A_1(LO) phonon peak at 565 cm^{-1} for as deposited ZnO:N film which is shifted to 567 cm^{-1} for film RTA at 400^{0}C and to 574 cm^{-1} for the film treated by RTA at 550^{0}C. These results are is in good agreement with the value found in the literature [24]. From the best fit we obtained the dielectric constants dispersion of the films (exemplified in Fig.9 f for the ZnO:N film after at RTA 550 ^{o}C)

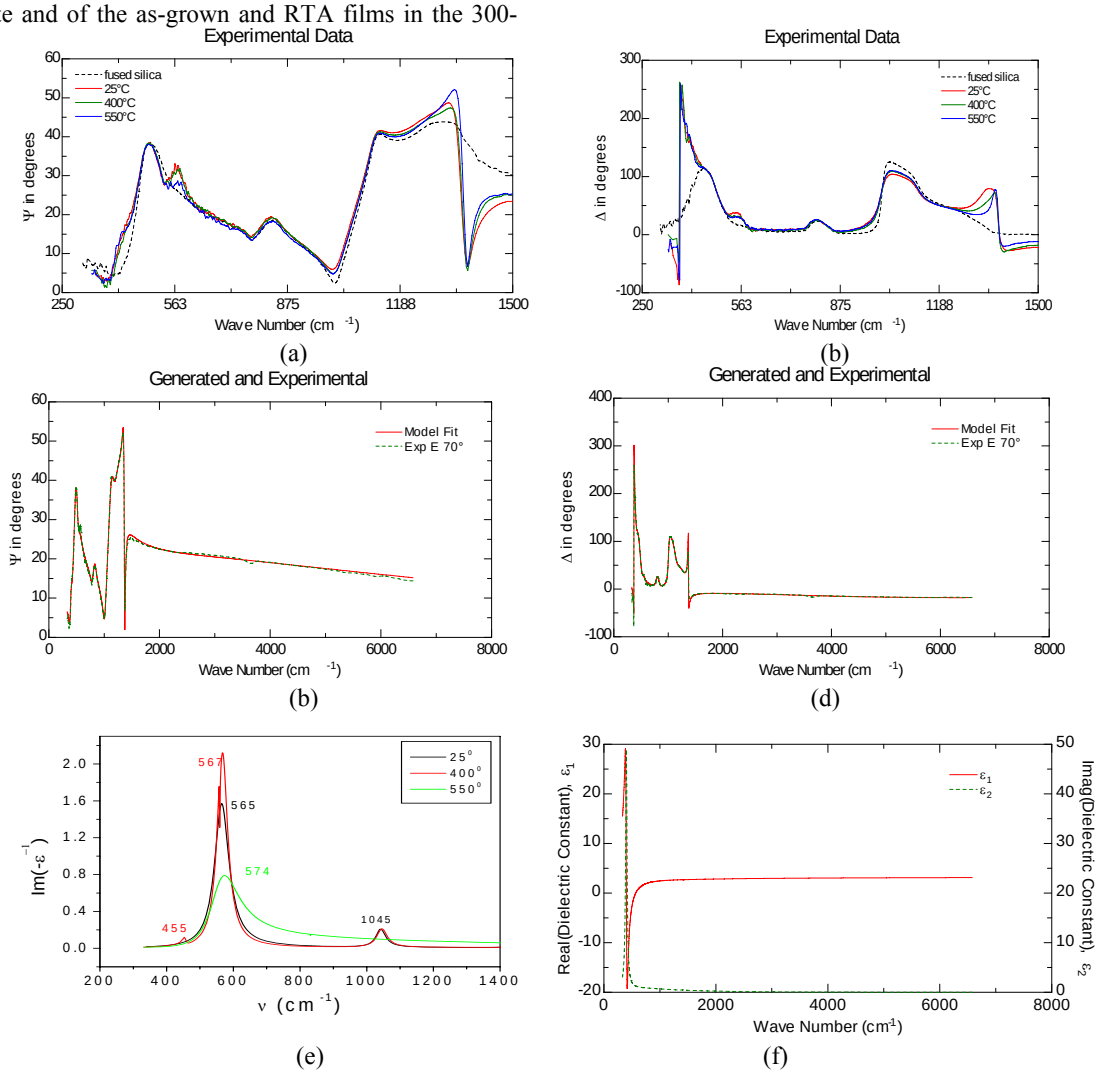

Fig. 9. Ellipsometric results of ZnO films in the IR range for as-deposited and RTA films: (a, b) - ellipsometric measurements; (c, d)- the agreement between the measured and computed data of ψ and Δ spectra for the sample RTA at 55 0^{0}C; (e)- imaginary part of the dielectric loss functions; (f) –dielectric constants.

The optical constants (n, k) of the as-deposited and RTA films determined separately in UV-VIS-NIR and in far IR spectral ranges were represented together in the Fig.10. A very good link was obtained between them in all three cases.

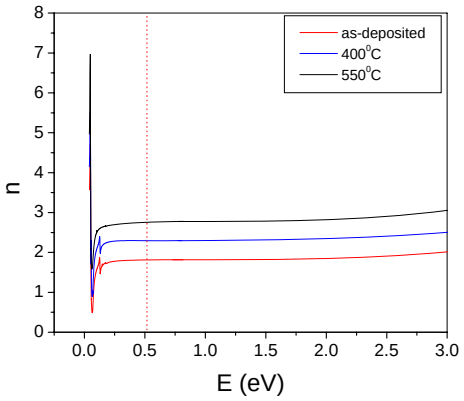

Fig.10 Optical constants of the as-deposited and RTA O:N films in UV-VIS-NIR-IR range

4. Conclusions

We report here on the surface topography and optical properties of the ZnO:N thin films formed by the rf magnetron sputtering using ZnN target (99.9% purity) on, unintentionally heated, glass substrates. The presence of the nitrogen in ZnO thin films is confirmed by the EDX measurements.

An improvement of the crystallinity and surface roughness of the ZnO:N thin films is found following RTA. We also noticed that the RTA do not reduce the ZnO:N thin films transparency in the Visible-NIR spectral range.

UV-VIS-NIR spectrophotometry and UV-VIS-NIR SE demonstrate that the improvement in the ZnO:N thin films crystallinity following RTA (observed by XRD) is accompanied by a slight decrease of the optical band gap and small increase of the film transparency.

The optical constant of ZnO:N thin films over a large spectral range (from UV to Far IR) and the active infrared modes are reported in this work.

Acknowledgements

This work was supported by the Irish SFI Strategic Research Cluster "FORME", Award number 07/SRC/I1172, the HEA PRLTI4 grant "INSPIRE" and partially supported by the Romanian PN2 project number 11061/2007."

References

[1] G. E. Jellison, L. A. Boatner, Phys. Rev. B **58**, 3586 (1998)

[2] D. P. Norton, Y. W. Heo, M. P. Ivill, K. Ip, S .J. Pearton, M. F. Chisholm, T. Steiner, Mater. Today **7**, 34 (2004)

[3] M. H. Huang, S. Mao, H. Feick, H. Yan, Y. Wu, H. Kind, E. Weber, R. Russo, P. Yang, Science **292**, 1897 (2001)

[4] H. Xu, X. Liu, D. Cui, M. Li, M. Jiang, Sensors Actuat B-Chem., **114**, 301 (2006)

[5] J. B. Baxter, E. S. Aydie, Sol. Energ. Mat. Sol. C. **90**, 607 (2006)

[6] E. M. C. Fortunato, P. M. C. Barquinha, A. C. M. B. G. Pimemtel, A.M.F. Gonçalves, A. J. S Marques, L. M. N. Pereira, R. Martins, Adv. Mater **17**, 590 (2005)

[7] A. C. Galca, M. Secu, A. Vlad, J. D. Pedarnig, Thin Solid Films (2010),doi:10.1016/j.tsf.2009.12.041

[8] L. S. Hsu, C. S. Yeh, C. C. Kuo, B. R. Huang, S. Dhar, J. Optoelectron. Adv. Mater. **7**(6), 3039 (2005)

[9] Y. Yan, S. B. Zhang, S. T. Pantelides, Phys. Rev. Lett. **86**, 25 (2001)

[10] S. B. Zhang, S.-H. Wei, A. Zunger, Phys. Rev. B **63**, 75205 (2001)

[11] Q. H. Li, D. Zhu, W. Liu, Y. Lui, X. C. Ma, Appl. Surf. Sci.**254**, 2922 (2008).

[12] A. Zunger, Appl. Phys. Lett. **83**, 57 (2003)

[13] T. Yamamoto, H. Katayama-Yoshida, Jpn. J. Appl. Phys.**38**, L166. (1999)

[14] L. G. Wang, A. Zunger, Phys. Rev. Lett. **90**, 256401 (2003).

[15] D. C. Look, B. Claflin, Phys. Status Solidi. B **3**, 624 (2004)

[16] V. S. Teodorescu, M. G. Blanchin, Microscopy and Microanalysis, **15**, 15 (2009)

[17] P. Sutta, Q. Jackuliak, Materials Structure, **5,** 10 (1998)

[18] M. Caglar, Y. Caglar, S. Ilican , J. Optoelectron. Adv. Mater. **8**(4), 1410 (2006)

[19] M. Nicolescu, M. Anastasescu, S. Preda, J. M. Calderon-Moreno, H. Stroescu, M. Gartner, V .S. Teodorescu, A. V. Maraloiu, V. Kampylafka, E. Aperathitis, M. Modreanu, J. Optoelectron. Adv. Mater., **12**(5),1045 (2010).

[20] F. K. Shan, Y. S. Yu, Thin Solid Films **435**, 174 (2003).

[21] P. Sagar, P. K. Shishodia, R. M. Mehra, H. Okada, A. Wakahara, A.Yoshida, J. Lumin. **126**, 800 (2007)

[22] A. Og. Dikovska, P. A. Atanasov, C. Vasileva, I. G. Dimitrov, T. R. Stoyanchov, J. Optoelectron. Adv. Mater. **7**(3), 1329 (2005)

[23] J. Tauc, R. Grigorovici, A. Vâncu, Phys. Status Solidi B **15**, 627 (1966).

[24] N. Ashkenov, B. N. Mbenkum, C. Bundesmann, V. Riede, M. Lorenz, D. Spemann, E. M. Kaidashev, A. Kasic, M. Schubert, M. Grundmann, J. Appl. Phys.**93**, 126 (2003).

*Corresponding author: mgartner@icf.ro